Materials Science

Volume 2, Issue 3, 230-242.
DOI: 10.3934/matersci.2015.230
Received date 12 May 2015,
Accepted date 11 August 2015,
Published date 18 August 2015

http://www.aimspress.com/

Research article

Aging dependent phase transformation of mesostructured titanium dioxide nanomaterials prepared by evaporation-induced self-assembly process: Implications for solar hydrogen production

Luther Mahoney, Shivatharsiny Rasalingam, Chia-Ming Wu, Rui Peng, and Ranjit T. Koodali*

Department of Chemistry, University of South Dakota, Vermillion, SD-57069, USA

* **Correspondence:** Email: Ranjit.Koodali@usd.edu; Tel: +1-605-677-6189; Fax: +1-605-677-6397.

Abstract: Mesostructured titanium dioxide materials were prepared by Evaporation-Induced Self-Assembly (EISA) method using titanium isopropoxide and a cationic surfactant. The titania phase could be tuned by simply varying the aging time. As the aging time increased, hierarchically structured mesoporous materials with mixed phases of titania were obtained. The rutile content was found to generally increase with length in aging time. The mesostructured materials were evaluated for hydrogen production, and a mixed phase consisting of 95% anatase and 5% rutile showed the highest activity. This study indicates that the aging time is an important parameter for the preparation of mesostructured materials with hierarchical porosities and mixed phase(s) of titania.

Keywords: evaporation-induced self-assembly; titanium dioxide; solar hydrogen; porous materials; phase transformation

1. Introduction

Titanium dioxide has been extensively investigated for applications ranging from water splitting, dye-sensitized solar cells, degradation of pollutants, and destruction of bacteria to bio-medical applications [1–5]. Titania has been widely used because it is inexpensive to synthesize, benign, and photostable. A porous structured titanium dioxide can improve photocatalytic activity due to improved mass transport properties. In this regard, mesoporous materials offer promise. In recent years, several methods have been attempted to prepare porous TiO_2 nanomaterials [6–8]. These

include supercritical, hydrothermal, hard templating, and Evaporation-Induced Self-Assembly (EISA) methods. The high temperature supercritical method minimizes the collapse of pores, but requires expensive instrumentation, is energy intensive, and has challenges in scaling up due to the requirements of relatively high pressures and temperatures [8]. Hydrothermal method requires the use of autoclaves and relatively high pressures and temperatures [9]. The hard templating method is laborious, requires multiple steps of impregnation and long processing times [10,11]. In comparison to the above methods, EISA seems to be a facile and simple method, and it has the added benefit that the materials can be prepared and processed at mild conditions [12,13]. Another main advantage of the EISA method is that the material can be recovered as a powder or as a film. Several parameters such as pH, water content, nature and concentration of precursor(s) and surfactant, humidity, temperature etc. affect the quality and nature of the final mesostructured material, and these have been investigated previously [6]. The common precursor(s) for the synthesis of titania by EISA include $TiCl_4$ and/or $Ti(OCH(CH_3)_2)_4$. $TiCl_4$ is highly reactive, toxic, and hazardous and hence titanium alkoxides are preferable. The EISA method involves the use of non-ionic (*e.g.* pluronic polymers such as P123) or cationic (*e.g.* cetyltrimethylammonium bromide (CTAB)) surfactants. An advantage of CTAB is that its critical micelle concentration is higher than that of P123. Also, the cloud point is a major issue with P123. Thus, a clear micellar solutions can be readily prepared at room temperature using CTAB. In addition, CTAB can be used at both low and high pH values. Thus, in the present study, $Ti(OCH(CH_3)_2)_4$ and CTAB were used in the preparation of TiO_2. Although several factors have been investigated, surprisingly, a systematic study of aging time has not been explored using the EISA method. This is important because the composition of the solution changes during the evaporation process, and this has profound effect on the nature of the final phase(s) formed.

It has been reported that mixed phases of titania exhibit higher activities in comparison to pure phases [14,15]. This has been the reason for the high activity of Degussa P25 for several photocatalytic reactions. Li et al. reported that the presence of small rutile crystallites in close contact with anatase created catalytic "hot spots" and this was responsible for high photocatalytic activity [16]. Thus, it is important to explore effective methods to prepare mixed-phase titania in a facile manner. Previous attempts to prepare TiO_2 with mixed phases using surfactants required calcination (typically at relatively high temperatures in the range of 600 to 1200 ^oC) [9], use of highly reactive $TiCl_4$ in addition to $Ti(OR)_4$ [17], or hydrothermal treatment [18]. In addition, microemulsion method [19], flame pyrolysis, [20], or physical vapor deposition [21] methods have also led to the formation of mixed phases of anatase and rutile. In comparison to these methods of synthesis, the EISA method seems to relatively easy.

The anatase-to-rutile phase transformation as a function of aging time for the preparation of TiO_2 mesostructured materials by the EISA method has not been investigated carefully and provides the impetus for this work. The mesostructured materials were evaluated for solar hydrogen production. The material with anatase (95%) and rutile (5%) exhibited high activity even in the absence of Pt as a co-catalyst. Our results suggest that mixed phases of TiO_2 with varying compositions can be obtained by aging using the EISA method and by calcination at moderate temperatures in contrast to previous literature attempts to prepare mixed phases of anatase and rutile. Thus, this synthetic protocol is simple, and the composition of the titania phase(s) can be varied by simply varying the aging time. This study provides an ideal opportunity for making both powders and thin films of mixed phases for various applications in a facile manner.

2. Materials and Methods

2.1. Materials

Commercially available cetyltrimethylammonium bromide (CTAB, Alfa Aesar, 98+%), titanium isopropoxide ($Ti(OCH(CH_3)_2)_4$, Acros, 98+%), conc. hydrochloric acid (Fisher-Scientific, ACS grade), ethanol (Pharmco-AAPER, ACS/USP grade, 200 proof) were used as received. Deionized water was used throughout the experiments.

2.2. Synthesis

The EISA method was used for preparing mesoporous TiO_2 materials [12,13,22]. In a typical synthesis, 0.468 g of cetyltrimethylammonium bromide (CTAB) was dissolved in 5 mL of ethanol in a beaker. The solution was heated slowly to 50 °C and the beaker was covered with parafilm to prevent evaporation of ethanol. In another beaker, 4.4 mL of ethanol, 2.4 mL of $Ti(OCH(CH_3)_2)_4$, and 0.93 mL of conc. HCl were mixed. These two solutions were combined and stirred. Then, 2.46 mL of deionized water was added drop wise and the mixture was stirred. The resulting solution was poured into petri dishes and then placed in an oven and heated to 60 °C and aged for various times. The materials were removed after 0.25, 1, and 6 days. Finally, the materials were calcined at 500 °C for 6 h in static air at a heating rate of 3 ^oC/min to remove the template and named as TiO_2-0.25d, TiO_2-1d, and TiO_2-6d.

Thermogravimetric analysis of the calcined mesostructured material indicates a weight loss of only 0.55 wt.% between 200 and 550 ^oC. This weight loss corresponds to loss of surface hydroxyl groups from titania, and this indicates that the cationic surfactant was removed after calcination.

2.3. Characterization and photocatalytic studies

TiO_2 materials were characterized extensively by a variety of techniques. The powder X-ray diffraction studies of the mesostructured materials were recorded at room temperature using a Rigaku Ultima IV instrument with Cu Kα radiation (λ = 1.5408 Å). The accelerating voltage used was 40 kV, and the emission current was maintained at 44 mA. The samples were scanned with a step size of 0.02°, in the 2θ range from 10 to 80°. The ratios of the mixed phases present in the samples were determined by performing quantitative analysis using the Reference Intensity Ratio (RIR) method in the PDXL software (version 2) provided by Rigaku. Raman spectra were collected using a Horiba Jobin Yvon Labram Aramis Raman spectrometer with a He-Ne laser (532 nm) as the light source. The unfiltered beam of scattered laser radiation was focused onto the materials using a microscope objective (×50) for an acquisition time of typically 10 s. Transmission Electron Microscopic (TEM) images were obtained using a Tecnai G^2 instrument operating at 120 kV. Prior to the analysis, the materials were dispersed in ethanol and the suspensions were sonicated for 30 min. Then, one drop of the suspension was placed on a copper grid coated with carbon film, and allowed to dry overnight before conducting the TEM studies. The textural properties, such as surface area, pore volume, and pore size distribution of the materials were analyzed using N_2 physisorption measurements. After the samples were dried overnight at 80 °C and degassed at 100 °C extensively, N_2 isotherms were obtained at −196 °C using a NOVA 2200e (Quantachrome Instruments) surface area analyzer. The

specific surface area was calculated by applying the Brunauer-Emmett-Teller (BET) equation to the relative pressure range (P/P_0) of 0.05–0.30. The pore volume was determined from the amount of N_2 adsorbed at the highest relative pressure of $P/P_0 \approx 0.99$. The average pore diameter was calculated by using the formula, average pore diameter = 4 (pore volume) / (specific surface area). The UV-Vis diffuse reflectance spectra were recorded using a Cary 100 Bio UV-Visible spectrophotometer equipped with a praying mantis diffuse reflection accessory (Harrick Scientific). The band gaps of the materials were calculated extrapolating the high slope region to the X-axis in the Tauc plot obtained by transforming the absorbance plot using the Kubelka-Munk function.

The photocatalytic experiments were carried out as follows. A known amount of the photocatalyst (1 g/L) was suspended in a solution of H_2O and methanol (molar ratio of $[H_2O]/[CH_3OH] = 8$). The suspension was degassed for 30 min. with high-purity argon prior to irradiation. The suspensions were continuously stirred throughout the course of the experiment. A 300 W Xenon lamp (Oriel light source) with an appropriate filter was used as the source of UV radiation. The amount of H_2 produced was measured by gas chromatography (SRI 8610 C) equipped with a molecular sieve column and a TCD detector, and by using a calibration curve prepared previously. Photoluminescence (PL) measurements were carried out on a Horiba Jobin Yvon-Fluoromax 4 instrument. The excitation wavelength used was 300 nm, and the emission spectra were monitored in the range of 375–500 nm.

3. Results and Discussion

The powder X-ray diffractograms of the titania materials as a function on aging is shown in Figure 1. After aging for 0.25 day, peaks due to (101), (103), (004), (112), (200), (105), (211), (213), (204), (116), (220), and (215) diffraction planes of the anatase phase only are observed.

After aging for 1 day, a small peak appears at $2\theta = 27.7^o$ that is due to (110) diffraction plane of the rutile phase. In addition, anatase phase which is predominant in this material can also be clearly seen. However, after 6 days of aging, the percentage of rutile increases significantly, and peaks due to (110), (101), (111), (210), (211), (220), (310), and (301) diffraction planes of rutile can be observed in addition to the anatase phase. The variation in the phase of titania can be explained as follows.

A typical EISA synthesis involves multiple steps, and the choice of the solvent, acid, amount of water, titania precursor, and surfactant is critical, apart from the aging temperature and time [7]. In the present work, the molar ratio of [water]/[titanium isopropoxide] used was relatively high, *i.e.* ~17. At such high ratios, both hydrolysis and condensation of the titania precursor occur rapidly. This leads to the formation of titania oxo clusters first, prior to self-assembly. As evaporation of the most volatile component (ethanol) takes place initially, there is an increase in the concentration of the titania oligomers and the non-volatile surfactant. This triggers the self-assembly process and leads to the formation of a titania-surfactant hybrid phase. The hybrid "titaniatropic" phase consists of pre-formed titania nanobuilding blocks that are self-assembled around the surfactant molecules. These interactions are of the type, $Ti^{-}OH+\ldots X-\ldots CTAB+$, where X represents bromide ions from CTAB, or chloride ions from HCl used in the synthesis. In the next steps, equilibration of water and solvent between the hybrid phase and the environment takes place. The continued evaporation of the solvent (ethanol and water) promotes the formation of a mesostructure. As the aging time is increased, the solution is progressively enriched with acid. Even though, most of the HCl eventually

evaporates, some amount of residual Cl^- ions persist leading to a condensed mesoporous network of the type $TiO_{2-x/2}(OH,Cl)_x$ [23]. It has been reported that as the acid concentration increases, the edge shared bonds between the titania octahedral clusters and oxygen atoms decreases and the corner shared bonds between the titania oxo clusters and oxygen increases [24,25]. In the rutile structure, each titania octahedron is linked to two edge shared and eight corner shared oxygen atoms, respectively. On the other hand, in the anatase structure, the titania octahedron are connected to four edge and four corner sharing oxygen pairs. The reorientation of the TiO_6 clusters due to the increase in the localized concentration of acid with aging time results in the formation of rutile phase. Hence, by changing the aging time, one can modulate the phase(s) of titania. In this study, the amount of rutile content continues to progressively increase with increase in aging time. For example, with an aging time of 6 h (TiO_2-0.25d), the rutile content was found to be 0% whereas after 6 days of aging (TiO_2-6d), a predominantly rutile phase (71%) was obtained. Further increase in aging time does not seem to increase the amount of rutile phase. For sake of briefness, we are discussing results pertaining to aging times of 6 h (TiO_2-0.25d), 1 day (TiO_2-1d), and 6 days (TiO_2-6d) in this study.

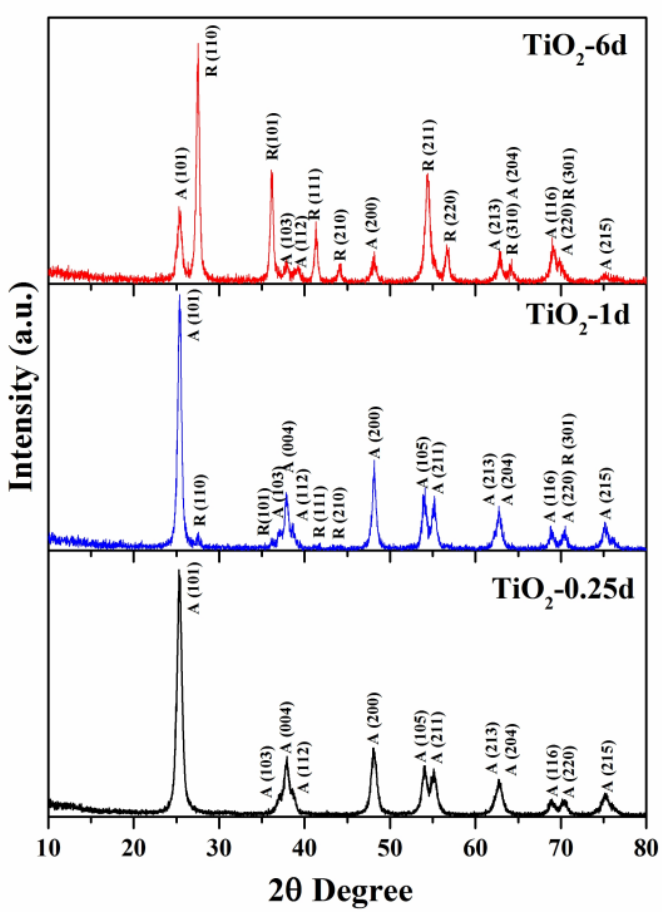

Figure 1. Powder X-ray diffractograms of mesostructured titanium dioxide.

Raman studies indicate the presence of only anatase in TiO_2-0.25d (Figure 2A) and is consistent with powder XRD studies. Peaks at 148 cm^{-1} (E_g), 393 cm^{-1} (B_{1g}), 519 cm^{-1} (A_{1g} and B_{1g}), and 643 cm^{-1} (E_g) attributed to the anatase phase can be clearly seen. Figure 2B shows the Raman spectra of TiO_2-1d. The highest intense peak seems to be slightly shifted to 143 cm^{-1} (E_g), whereas the other

peaks appear at wavenumbers similar to those observed in TiO_2-0.25d. However, the Raman spectra of TiO_2-1d show phonon modes due to the anatase phase only. This may be due to the relatively low amounts of rutile (5%) and sensitivity of the instrument that preclude the observation of phonon modes of rutile. However, the material aged after 6 days, TiO_2-6d show peaks due to both anatase and rutile phases. In addition to the phonon modes of anatase described previously for TiO_2-0.25d and TiO_2-1d, peaks at 230 cm^{-1} (E_g), 442 cm^{-1} (E_g), and 610 cm^{-1} (A_{1g}) that may be ascribed to the rutile phase can also be seen as indicated in Figure 2C. Thus, the Raman studies confirm the findings of the powder XRD studies.

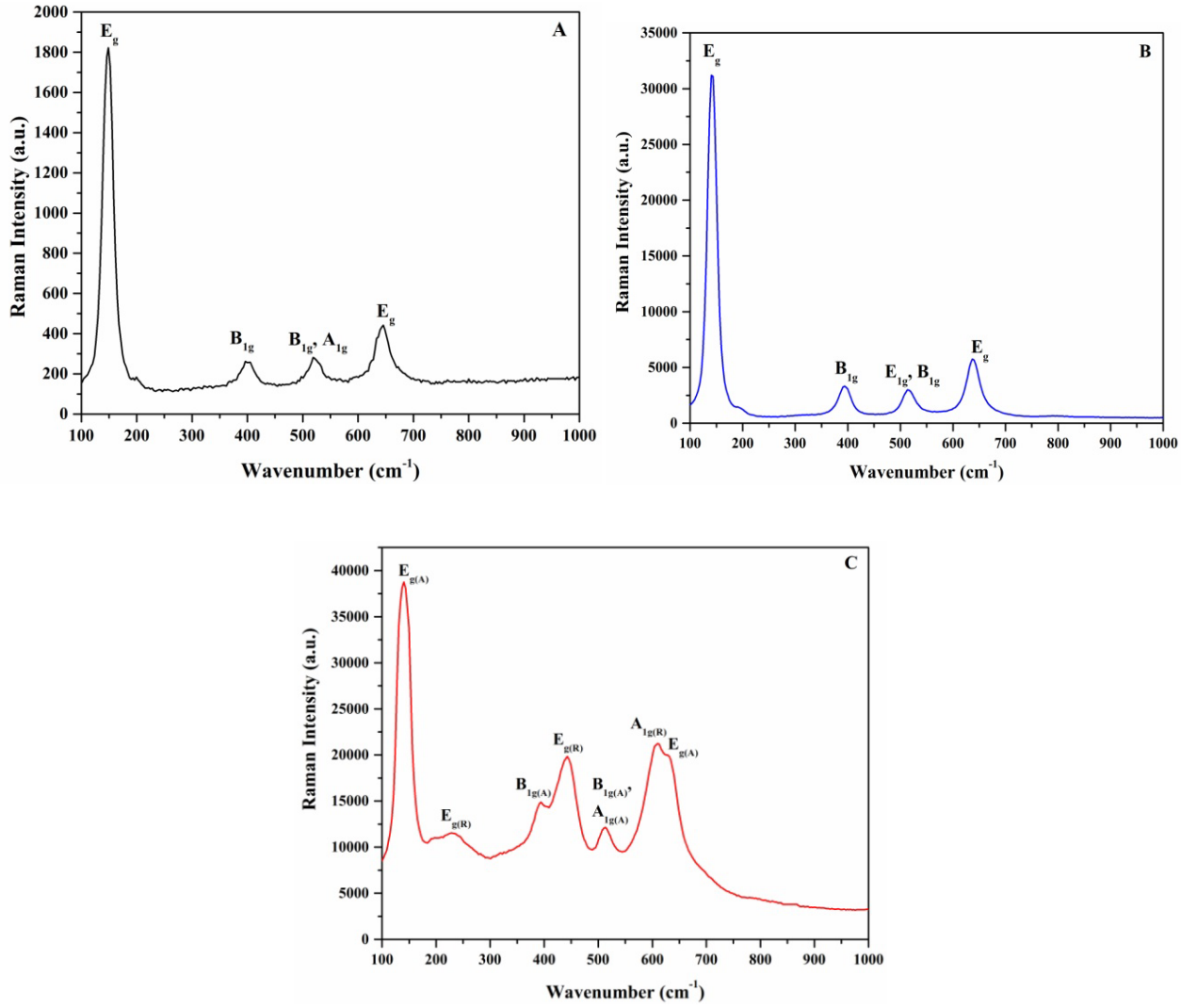

Figure 2. Raman spectra of A) TiO_2-0.25d, B) TiO_2-1d, and C) TiO_2-6d. A and R in Figure 2C denote anatase and rutile phases respectively.

Transmission electron microscopic (TEM) studies were also conducted to discern the morphology and phase. The TEM image of TiO_2-0.25d shown in Figure 3A, indicate the presence of irregularly shaped titania particles that are fairly compact in nature, *i.e.* less porous in nature. The high resolution TEM images are shown in the inset in Figure 3A. Lattice fringes with *d* spacing values of 3.50 Å can be seen. This value is close to the *d* spacing (3.52 Å) of the (101) plane that is

predominant in anatase. The TEM of TiO_2-6d (Figure 3B) indicate a more open porous structure. The inset in Figure 3B shows the presence of both anatase (due to *d* (101) with a value of 3.50 Å) and rutile (due to *d* (110) with a value of 3.23 Å) phases, and is consistent with powder XRD and Raman studies. In summary, powder XRD, Raman, and TEM studies indicate the presence of a mixed phase in the sample aged for 6 days, whereas only anatase phase is present after 6 hours of aging. Aging for 1 day results in the presence of small amounts (5 wt.%) of rutile phase, which can be discerned from powder XRD studies only.

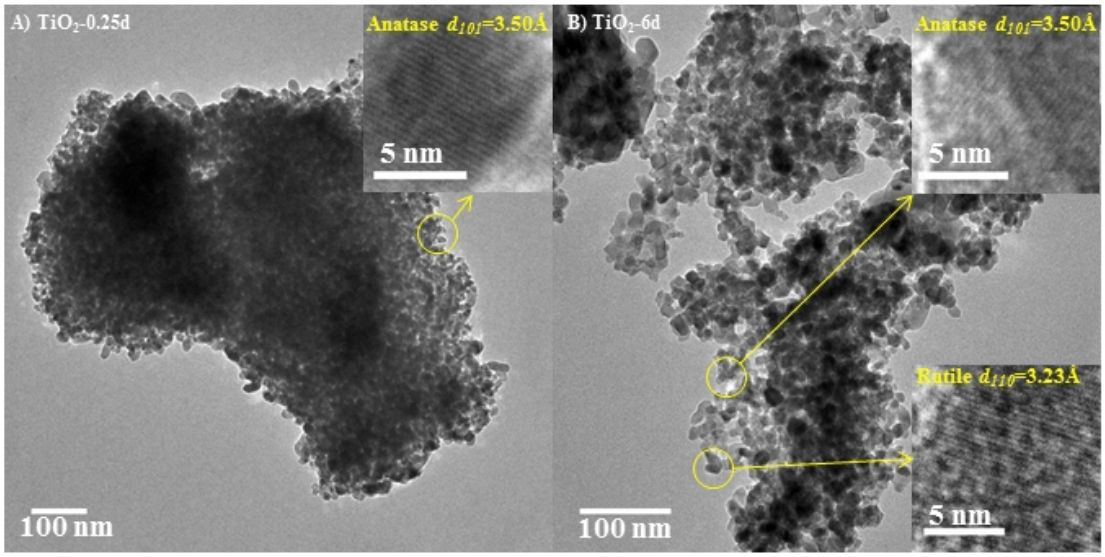

Figure 3. Transmission electron microscopic images of A) TiO_2-0.25d and B) TiO_2-6d.

The textural properties of the mesostructured materials were investigated, and the results are shown in Figure 4. The materials exhibit type IV (IUPAC classification) isotherms, which are typical of mesoporous materials.

Figure 4A shows the nitrogen isotherm for TiO_2-0.25d. At low values of relative pressures (P/P_0), monolayer adsorption of N_2 takes place. This is followed by multilayer adsorption and capillary condensation at higher relative pressures. Owing to the differences in pressures at which capillary evaporation and condensation take place, the isotherms display hysteresis. The hysteresis observed in this material, can be classified as H1 type. This type of hysteresis loop is typical of materials that contain aggregates that are fairly compact and having high degree of pore uniformity [26]. The pore volume (0.15 cm^3/g) and specific surface area (72 m^2/g) of this material is relatively low. The inset in Figure 4A shows the pore size distribution. As can be seen in the inset, the pore size is fairly uniform and centered near 80 Å. On increasing the aging time to 1 day, the specific surface area increases dramatically from 72 m^2/g (for the sample, TiO_2-0.25d) to 161 m^2/g in TiO_2-1d. The isotherm (Figure 4B) indicates that the hysteresis loops do not level off at relative pressures close to the saturation vapor pressure, suggesting that the materials are composed of loose assemblies of irregular shaped plate-like particles forming slit-like pores of broad pore size distribution. The broad pore size distribution can be seen in the inset in Figure 4B. A hierarchical set of pores centered near 50 Å and 100 Å, and extending into the upper range of mesopore (500 Å) can be observed. Increasing the aging time to 6 days, preserves the mesoporosity and the specific surface area drops

slightly to 145 m^2/g. However, the pore volume is still large. The isotherm and the pore size distribution for TiO_2-6d is shown in Figure 4C. The results are similar to that observed for the sample aged for 1 day, *i.e.*, TiO_2-1d. The textural properties of the mesostructured materials are listed in Table 1. In summary, the textural properties of the mesostructured materials indicate that extending the aging time facilitates in creating more open and porous mesostructures with higher specific surface area and larger pore volumes.

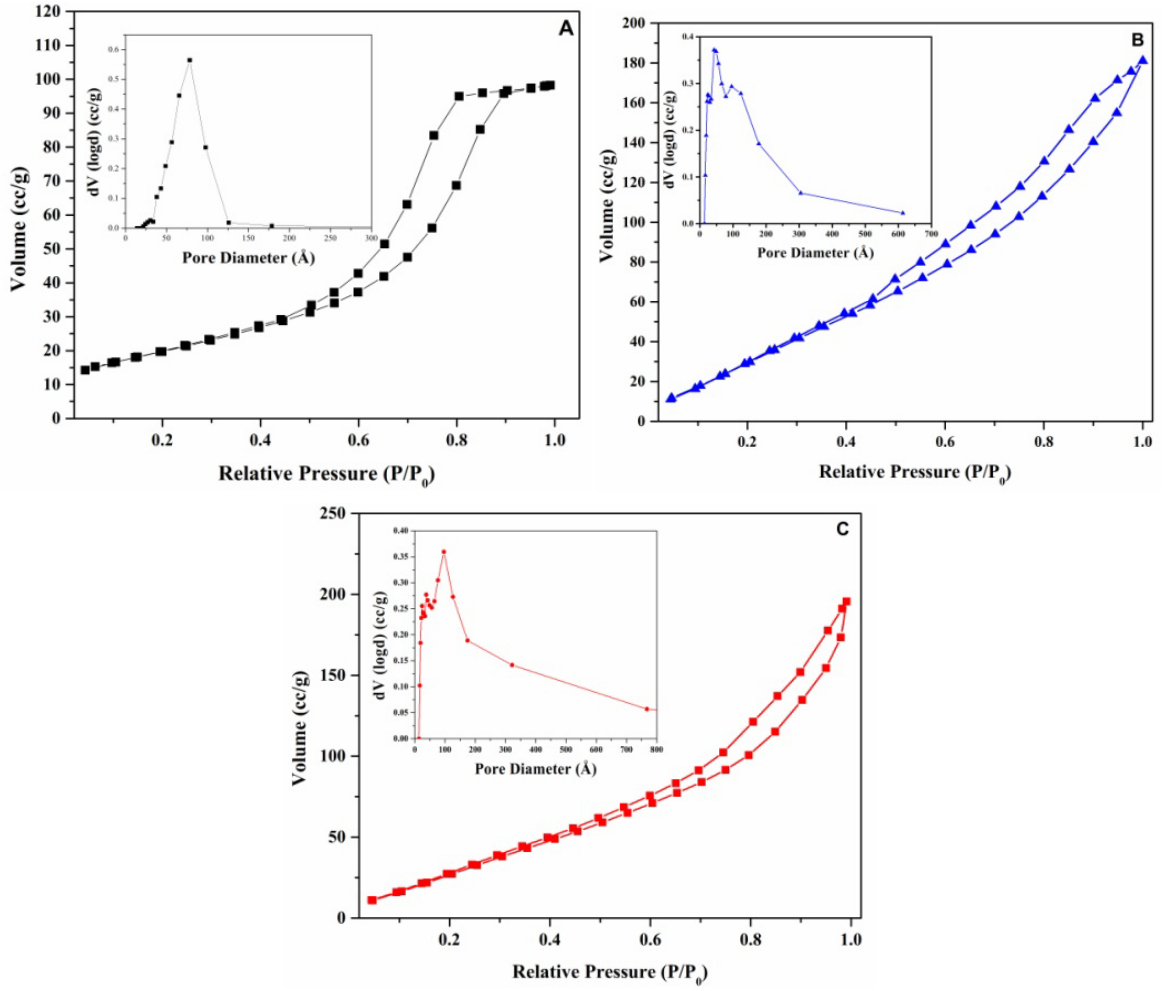

Figure 4. Nitrogen physisorption isotherms of A) TiO_2-0.25d, B) TiO_2-1d, and C)TiO_2-6d. The pore size distribution plots are shown in the inset.

Diffuse reflectance (DR) spectral studies were carried out in order to discern the band gap. The absorption edge was calculated by plotting the Kubelka-Munk function, $[KE]^{1/2}$ against the photon energy, E, measured in eV (Figure 5). The band gap energy (E_g) was estimated by extrapolating the linear portion of the spectra to $[KE]^{1/2} = 0$. The DRS studies indicate that the band gap decreases as the rutile content increases, as indicated in Table 1. This is consistent with the fact that the band gap of anatase and rutile are ~3.2 and ~3.0 eV, respectively. Increase in the aging time increases the amount of rutile, and the DRS results obtained in this study are consistent with the expected trend.

Table 1. Physico-chemical properties of titanium dioxide prepared at various aging times.

Material	Anatase Crystallite Size (nm)[a]	Anatase (%)[b]	Rutile (%)[b]	Specific Surface Area (m^2/g)[c]	Pore Volume (cc/g)[d]	Average Pore Diameter (Å)	Bandgap (eV)[f]	H_2 (mmole /g TiO_2)
TiO_2-0.25d	10	100	0	72	0.15	84	3.22	0.27
TiO_2-1d	16	95	5	161	0.28	70	3.09	0.51
TiO_2-6d	13	29	71	145	0.30	83	3.04	0.09

[a] Crystallite size was calculated using the Debye-Scherrer method by selecting the highest intense peak for anatase at $2\theta = 25.36°$ (d_{101}).

[b] TiO_2 phase percentages were calculated using reference intensity ratio (RIR) using the Rigaku PDXL software.

[c] Specific surface area was determined by applying the Brunauer-Emmett-Teller (BET) equation to the relative pressure range of $P/P_0 = 0.05–0.30$.

[d] The pore volume was determined from the amount of N_2 adsorbed at the highest relative pressure (P/P_0) of approximately 0.99.

[e] The bandgap was estimated by extrapolation of the high slope value from the Kubelka-Munk plot on the X-axis.

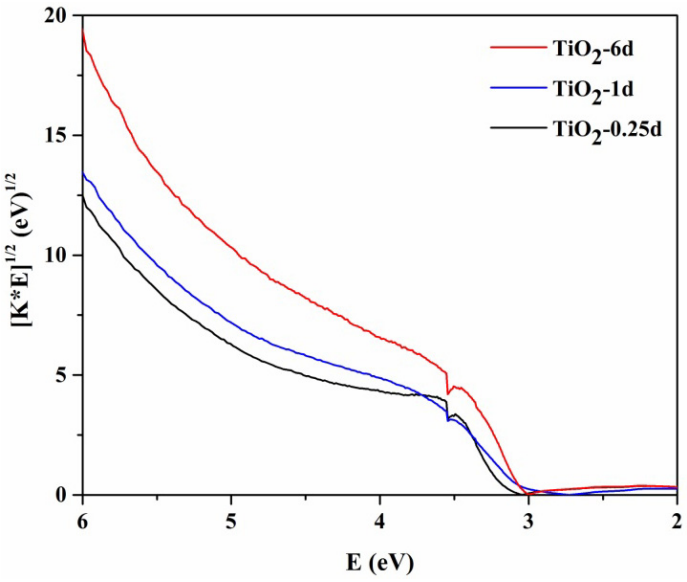

Figure 5. Tauc plots (obtained by transformation of the Kubelka-Munk equation) for the mesostructured titanium dioxide materials.

The photocatalytic activity of the materials was investigated, and the results are shown in Figure 6. After four hours of irradiation, the activity is found to be in the order TiO_2-1d > TiO_2-0.25d > TiO_2-6d.

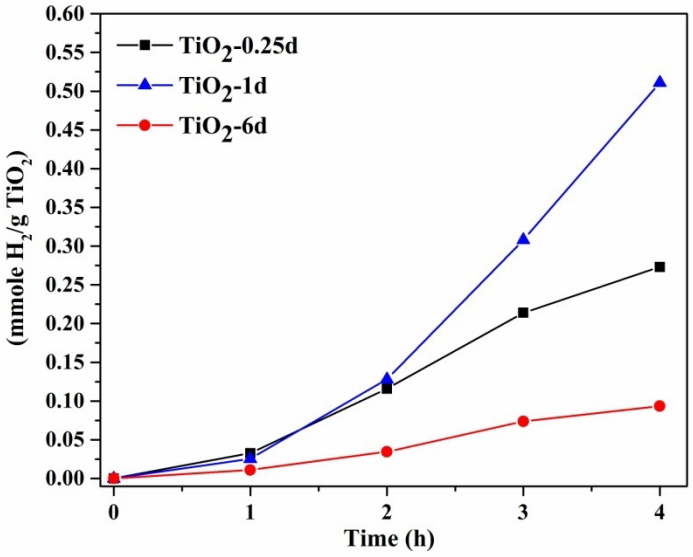

Figure 6. Variation in hydrogen yields for the mesostructured titanium dioxide materials.

TiO_2-1d has 95% anatase and 5% rutile phases, whereas TiO_2-0.25d has only anatase phase. TiO_2-6d showed 29% anatase and 71% rutile. The conduction band edge of rutile is relatively more positive as compared to anatase, and the presence of excess rutile content is detrimental to photocatalytic activity [14]. These results suggest an optimal amount of rutile is conducive to enhanced activity.

The photocatalytic activity of TiO_2 is dependent on the crystallinity, crystallite size, surface area, porosity, phase etc. Even though the crystallinity of TiO_2-0.25d is higher than that of other materials prepared in this study, its activity is lower in comparison to the material, TiO_2-1d. This may be due to its relatively low surface area. The crystallite sizes of the materials lie in a narrow range and cannot account for the differences in activity. The high activity of TiO_2-1d may be attributed to its high specific surface area and most importantly because of the presence of an optimal amount of mixed phases of anatase and rutile that minimizes electron-hole recombination. The presence of mixed phases of titania has been shown to have important implications in photocatalysis. The synergistic effect in the material, TiO_2-1d is due to the effective trapping and separation of the charge-carriers across the two different crystallite phases [14]. This has been observed previously and our results are consistent with prior observations.

In order to understand the trends in photocatalytic activities, photoluminescence (PL) studies were carried out. PL experiments (Figure 7) confirm the trends in photocatalytic activities. TiO_2-1d shows the least emission indicating that the recombination of electron-hole pairs are minimized the most in this material.

TiO_2-6d show higher emission indicating enhanced recombination of the charge-carriers. The high rate of recombination of the charge-carriers results in low activity and the presence of large amounts of rutile is detrimental to its activity because its conduction band is located at relatively more positive values to the H^+/H_2 redox couple. The emission observed in the mesostructured titania materials are the characteristic emissions due to the recombination of free and bound excitons.

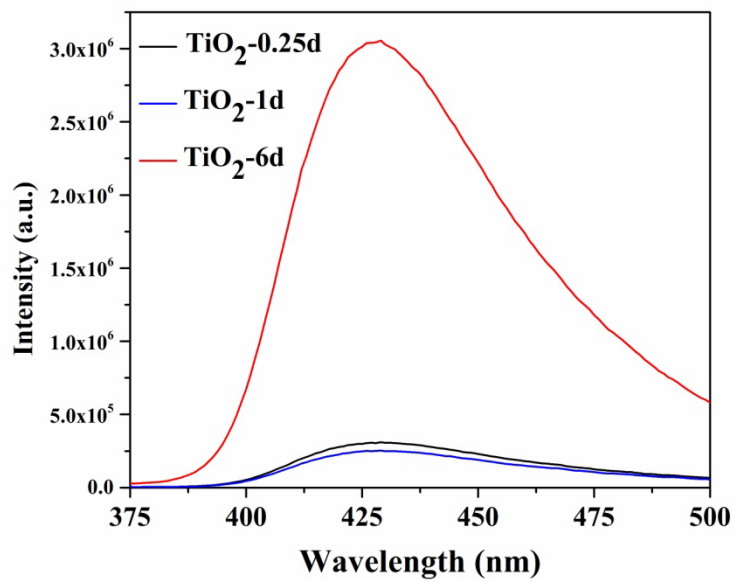

Figure 7. Photoluminescence spectral emissions from the mesostructured titanium dioxide materials.

4. Conclusion

EISA is a versatile method for the preparation of hierarchical mesostructured TiO_2. By changing the aging time, one can successfully prepare controlled amounts of mixed phases by using a convenient titania precursor and a readily available surfactant. A mixed mesostructured titania consisting of anatase (95%) and rutile (5%) showed high photocatalytic activity due to minimized electron-hole recombination and enhanced specific surface area. This facile method paves the way for the fabrication of hierarchical porous TiO_2 for other applications such as degradation of dyes.

Acknowledgments

This work was supported by DE-EE-0000270, NSF-CHE-0722632, NSF-CHE-0840507, NSF-DGE-0903685, NSF-EPS-0903804, and SD NASA-EPSCOR NNX12AB17G. We are thankful to Dr. C.Y. Jiang for Raman studies.

Conflict of Interest

The authors declare no conflicts of interest in this paper.

References

1. Bai J, Zhou BX (2014) Titanium dioxide nanomaterials for sensor applications. *Chem Rev* 114: 10131–10176.
2. Bai Y, Mora-Sero I, De Angelis F, et al. (2014) Titanium dioxide nanomaterials for photovoltaic applications. *Chem Rev* 114: 10095–10130.

3. Ma Y, Wang XL, Jia YS, et al. (2014) Titanium dioxide-based nanomaterials for photocatalytic fuel generations. *Chem Rev* 114: 9987–10043.
4. Sang LX, Zhao YX, Burda C (2014) TiO_2 nanoparticles as functional building blocks. *Chem Rev* 114: 9283–9318.
5. Schneider J, Matsuoka M, Takeuchi M, et al. (2014) Understanding TiO_2 photocatalysis: mechanisms and materials. *Chem Rev* 114: 9919–9986.
6. Soler-Illia GJdAA, Sanchez C, Lebeau B, et al. (2002) Chemical strategies to design textured materials: from microporous and mesoporous oxides to nanonetworks and hierarchical structures. *Chem Rev* 102: 4093–4138.
7. Shen X, Zhang J, Tian B (2011) Microemulsion-mediated solvothermal synthesis and photocatalytic properties of crystalline titania with controllable phases of anatase and rutile. *J Hazard Mater* 192: 651–657.
8. Parayil SK, Psota RJ, Koodali RT (2013) Modulating the textural properties and photocatalytic hydrogen production activity of TiO_2 by high temperature supercritical drying. *Int J Hydrogen Energ* 38: 10215–10225.
9. You X, Chen F, Zhang J (2005) Effects of calcination on the physical and photocatalytic properties of TiO_2 powders prepared by sol-gel template method. *J Sol-Gel Sci Techn* 34: 181–187.
10. Hwang K-J, Yoo S-J, Kim S-S, et al. (2008) Photovoltaic performance of nanoporous tio_2 replicas synthesized from mesoporous materials for dye-sensitized solar cells. *J Nanosci Nanotechno* 8: 4976–4981.
11. Hwang K-J, Shim W-G, Jung S-H, et al. (2010) Analysis of adsorption properties of N719 dye molecules on nanoporous TiO_2 surface for dye-sensitized solar cell. *Appl Surf Sci* 256: 5428–5433.
12. Cassiers K, Linssen T, Meynen V, et al. (2003) A new strategy towards ultra stable mesoporous titania with nanosized anatase walls. *Chem Comm* 21: 1178–1179.
13. Meynen V, Cool P, Vansant EF (2009) Verified syntheses of mesoporous materials. *Micropor Mesopor Mat* 125: 170–223.
14. Kho YK, Iwase A, Teoh WY, et al. (2010) Photocatalytic H_2 Evolution over TiO_2 nanoparticles. The synergistic effect of anatase and rutile. *J Phys Chem C* 114: 2821–2829.
15. Andronic L, Perniu D, Duta A (2013) Synergistic effect between TiO_2 sol-gel and Degussa P25 in dye photodegradation. *J Sol-Gel Sci Techn* 66: 472–480.
16. Li G, Dimitrijevic NM, Chen L, et al. (2008) The important role of tetrahedral Ti^{4+} sites in the phase transformation and photocatalytic activity of TiO_2 nanocomposites. *J Am Chem Soc* 130: 5402–5403.
17. Chen L, Yao B, Cao Y, et al. (2007) Synthesis of well-ordered mesoporous titania with tunable phase content and high photoactivity. *J Phys Chem C* 111: 11849–11853.
18. Dai S, Wu Y, Sakai T, et al. (2010) Preparation of highly crystalline TiO_2 nanostructures by acid-assisted hydrothermal treatment of hexagonal-structured nanocrystalline titania/cetyltrimethyammonium bromide nanoskeleton. *Nanoscale Res Lett* 5: 1829–1835.
19. Yan M, Chen F, Zhang J, et al. (2005) Preparation of controllable crystalline titania and study on the photocatalytic properties, *J Phys Chem B* 109: 8673–8678.
20. Teleki A, Pratsinis SE, Kalyanasundaram K, et al. (2006) Sensing of organic vapors by flame-made TiO_2 nanoparticles. *Sensor Actuat B-Chem* 119: 683–690.

21. Meyer S, Gorges R, Kreisel G (2004) Preparation and characterisation of titanium dioxide films for catalytic applications generated by anodic spark deposition. *Thin Solid Films* 450: 276–281.
22. Grosso D, Cagnol F, Soler-Illia G, et al. (2004) Fundamentals of mesostructuring through Evaporation-Induced Self-Assembly. *Adv Funct Mater* 14: 309–322.
23. Crepaldi EL, Soler-Illia GJdAA, Grosso D, et al. (2003) Controlled formation of highly organized mesoporous titania thin films: From mesostructured hybrids to mesoporous nanoanatase TiO_2. *J Am Chem Soc* 125: 9770–9786.
24. Wang C-C, Ying JY (1999) Sol−Gel synthesis and hydrothermal processing of anatase and rutile titania nanocrystals. *Chem Mater* 11: 3113–3120.
25. Yanagisawa K, Ovenstone J (1999) Crystallization of anatase from amorphous titania using the hydrothermal technique: Effects of starting material and temperature. *J Phys Chem B* 103: 7781–7787.
26. Kruk M, Jaroniec M (2001) Gas adsorption characterization of ordered organic−inorganic nanocomposite materials. *Chem Mater* 13: 3169–3183.

AIMS Press